Formation of a Positive Fixed Charge at c-Si(111)/a-$Si_3N_{3.5}$:H Interfaces

L. E. Hintzsche,[1] C. M. Fang,[1] M. Marsman,[1] M. W. P. E. Lamers,[2] A. W. Weeber,[2] and G. Kresse[1]

[1]*University of Vienna, Faculty of Physics and Center for Computational Materials Science, Sensengasse 8/12, A-1090 Vienna, Austria*

[2]*ECN Solar Energy, P.O. Box 1, 1755 ZG Petten, The Netherlands*

(Received 16 January 2015; revised manuscript received 5 April 2015; published 11 June 2015)

Modern electronic devices are unthinkable without the well-controlled formation of interfaces at heterostructures. These structures often involve at least one amorphous material. Modeling such interfaces poses a significant challenge, since a meaningful result can be expected only by using huge models or by drawing from many statistically independent samples. Here we report on the results of high-throughput calculations for interfaces between crystalline silicon (c-Si) and amorphous silicon nitride (a-$Si_3N_{3.5}$:H), which are omnipresent in commercially available solar cells. The findings reconcile only partly understood key features. At the interface, threefold-coordinated Si atoms are present. These are caused by the structural mismatch between the amorphous and crystalline parts. The local Fermi level of undoped c-Si lies well below that of a-SiN:H. To align the Fermi levels in the device, charge is transferred from the a-SiN:H part to the c-Si part resulting in an abundance of positively charged, threefold-coordinated Si atoms at the interface. This explains the existence of a positive, fixed charge at the interface that repels holes.

DOI: 10.1103/PhysRevApplied.3.064005

I. MOTIVATION

Silicon is the most important material for single-junction solar cells. Although there are other promising compounds for photovoltaic devices such as GaAs, CdTe, or InP, silicon-based cells still maintain about 90% market share [1,2]. Silicon has the advantage of being widely available, nontoxic, and applicable to many different requirements. The possible applications range from less efficient, but cheap, amorphous cells over cost-efficient multicrystalline cells up to highly efficient, but more expensive, monocrystalline cells [1,3]. To produce high-performance cells, optical losses must be minimized and recombination centers passivated. Meeting both challenges, amorphous silicon nitride (a-SiN:H) is commonly deposited as an antireflection and passivation layer on top of crystalline silicon (c-Si) solar cells with a p-type base and n-type emitter. Using plasma-enhanced chemical vapor deposition [4,5], the deposition parameters (i.e., the gas mixture of N_2-SiH_3 or NH_3-SiH_3) control the refractive index as well as the defect concentration of a-Si_3N_x:H so that the reflectivity and the passivation can be tuned for optimal cell performance.

However, even with high-quality surface passivation, the defect concentration at interfaces is larger than in bulk materials, and defect-assisted Shockley-Read-Hall recombination remains a major source of carrier losses in solar cells [6,7]. In particular, defect levels in the middle of the Si band gap are effective recombination centers and carrier traps. They reduce the lifetime of electron-hole pairs in c-Si and, therewith, the efficiency of the solar cells [8,9]. Lamers *et al.* [10] showed that the defect density correlates with what is called the "fixed charge." This fixed charge is positive and located at the c-Si/a-SiN:H interface. In contrast to charge-neutral recombination centers, the fixed charge increases the lifetime of charge carriers in n-doped c-Si by repelling holes from the interface. As undercoordinated Si atoms can have negative, neutral, or positive charge (i.e., K^-, K^0, or K^+ defects), the fixed charge is typically explained by an increased number of K^+ defects at the interface [11]. However, it is still unclear how those defects form and whether one could also produce c-Si/a-SiN:H interfaces with a negative, fixed charge that repels electrons and attracts holes. It is, therefore, obvious that defects are important to understand the properties of c-Si/a-SiN:H interfaces. Nonetheless, they are very difficult to investigate by experimental methods alone. For instance, lifetime measurements estimate defect concentrations indirectly, and electron spin resonance measurements can solely detect states occupied by a single electron [12].

For this reason, several authors recently examined c-Si/a-SiN:H interfaces by using computer simulations [13–20]. For example, Butler *et al.* [15,16] performed a topological analysis and compared the density of structural defects for different thicknesses of the transition region between c-Si and a-SiN:H. The study suggests an optimal thickness of 2 nm; however, a computationally cheap Tersoff potential was used and, like other studies employing force-field methods [13], their work was limited to investigations of structural properties. Specifically, their conclusions on electronic properties were based on the assumption that all undercoordinated atoms are recombination centers. As the electronic properties are important for most applications, *ab initio* methods seem to be more suitable. Pham *et al.* [20] generated c-Si/a-SiN:H

interface structures by combining classical molecular dynamics and *ab intio* methods. Afterwards, they examined the G_0W_0 corrected band offsets and the change of the dielectric constant perpendicular to the interface. Their focus was clearly on the application of *a*-SiN:H as a high-*K* dielectric in MOS-FET devices, since recombination centers were not examined in their work.

II. MODELING SETUP

In the present paper, we explicitly investigate the electronic properties of gap states at *c*-Si/*a*-$Si_3N_{3.5}$:H interfaces with 1- and 11-at. % hydrogen (H). The undoped *c*-Si part is modeled by a hexagonal $\sqrt{7} \times \sqrt{7}$ unit cell containing four double layers of seven Si atoms stacked in the (1 1 1) direction with a corresponding lattice constant of $a = 5.43$ Å. The cell volume of the crystalline part is 20.03 $Å^3$/atom with a density of 2.32 g cm^{-3}. The *a*-SiN:H part is made up by 59 Si, 69 N, and 1 or 17 H atoms. This composition is commonly used for photovoltaic applications and has a typical refractive index between 2.0 and 2.1 [18]. The volume corresponding to the amorphous part is 1429 $Å^3$ with a respective density of 3.04 or 3.06 g cm^{-3}. We also investigate 4×4 unit cells with six Si double layers of 16 Si atoms finding virtually identical results.

Since defects are minority species which are difficult to describe using force fields, our study uses a large-scale *ab initio* molecular-dynamics approach based on density-functional theory (DFT). Specifically, we use the Vienna *Ab Initio* Simulation Package and the projector-augmented-wave (PAW) method [21–23]. The PAW potentials of Si and N are softened to allow for a rather low plane-wave basis set corresponding to a cutoff energy of about 150 eV. In accordance with our previous studies [24,25], we apply the exchange correlation functional that was suggested by Perdew, Burke, and Ernzerhof and optimized for solids and surfaces (PBEsol) [26]. Periodic boundary conditions are applied as well. During the molecular-dynamics simulations, we use a time step of 1.5 fs and a Nose thermostat [27,28] to model a canonical ensemble. All finite-temperature simulations are performed with a *k*-point sampling restricted to the Γ point.

The preparation process of the interface samples is divided into several steps. As a starting configuration, we choose an already molten crystalline Si_3N_4 structure with Si, N, and H atoms that are added or removed in order to create the desired system composition [24]. Next, we generate a melt of *a*-$Si_3N_{3.5}$:H without *c*-Si by performing a 15-ps molecular-dynamics simulation at 4000 K. Then we rapidly reduce the temperature to 2500 or 2700 K, which is still above the onset of amorphization for 11- and 1-at. % H, respectively [24]. After 7.5-ps equilibration time, we start a long simulation at the same temperature lasting for 225 ps. From the resulting trajectory, we then draw 30 bulk *a*-$Si_3N_{3.5}$:H samples with an effective time difference of 7.5 ps between each sample. The extracted samples are combined with bulk *c*-Si to form 30 initial interface structures. These structures are first briefly equilibrated for 4.5 ps at 2500 or 2700 K, and then a 45-ps molecular-dynamics simulation is performed for each interface sample at the same temperature. From each trajectory of the 30 interfaces, we eventually extract three interface samples with an effective time difference of 15 ps between each sample. By cooling all 30×3 interface structures from the melt (2500–2700 K) to the amorphous state (1500 K) in 37.5 ps, we obtain 90 nearly independent sample structures for both system compositions. All samples are relaxed and finally recalculated with an $8 \times 8 \times 1$ *k*-point grid.

To compensate for the lack in system size, we average over the microscopic configurations. We examine the electronic gap states and link them to the geometrical properties of the structures [25]. For the band-structure analysis, we examine the hexagonal Brillouin zone by going from Γ (0, 0, 0) to *M* ($\frac{1}{2}$, 0, 0), from *M* to *K′* ($\frac{1}{3}$, $-\frac{1}{3}$, 0), and from *K′* to Γ. Before we continue with the results, we note that our interfaces are sharp. This is achieved by keeping the *c*-Si atoms partially fixed by allowing only for in-plane movements at the interface. Eventually, we remove this restriction at the interface in the final relaxation step.

III. RESULTS

A. Spatial location of gap states

In the following, we summarize our most important results by investigating the layer-resolved number densities and the electronic density of states (DOS) at the *c*-Si/*a*-$Si_3N_{3.5}$:H interface (Fig. 1). The structural mismatch causes slight distortions in the first double layer of *c*-Si, and, more important, long-range density fluctuations in the *a*-SiN:H part, with a pronounced increase in the N density around 1.7 Å [Fig. 1(a), red lines] above the Si topmost layer. These N atoms always bind to Si surface atoms, saturating 60% of the Si surface dangling bonds. The other Si surface atoms bind to Si atoms in the amorphous part. This causes the onset of a peak in the Si number density. The corresponding peak integrates to 1.3 Si atoms per Si surface atom, and the region is unusually Si rich, with very little N content. An analysis of the bonding topology suggests that a large number of threefold-coordinated Si K defects exist in this region, similar to but in much greater number than in bulk *a*-SiN:H [25]. These geometrical defects also cause a large number of electronic defect levels located in the band gap of *c*-Si [Fig. 1(b), region (iii)]. On the *c*-Si side, our analysis at first sight also suggests a large number of defect levels [Fig. 1(b), region (ii)]; however, an inspection of the charge density of these states indicates that these are conduction-band-like *c*-Si states (red arrow). We note that an analysis of the large 4×4 unit cell yields *quantitatively* identical results (not shown).

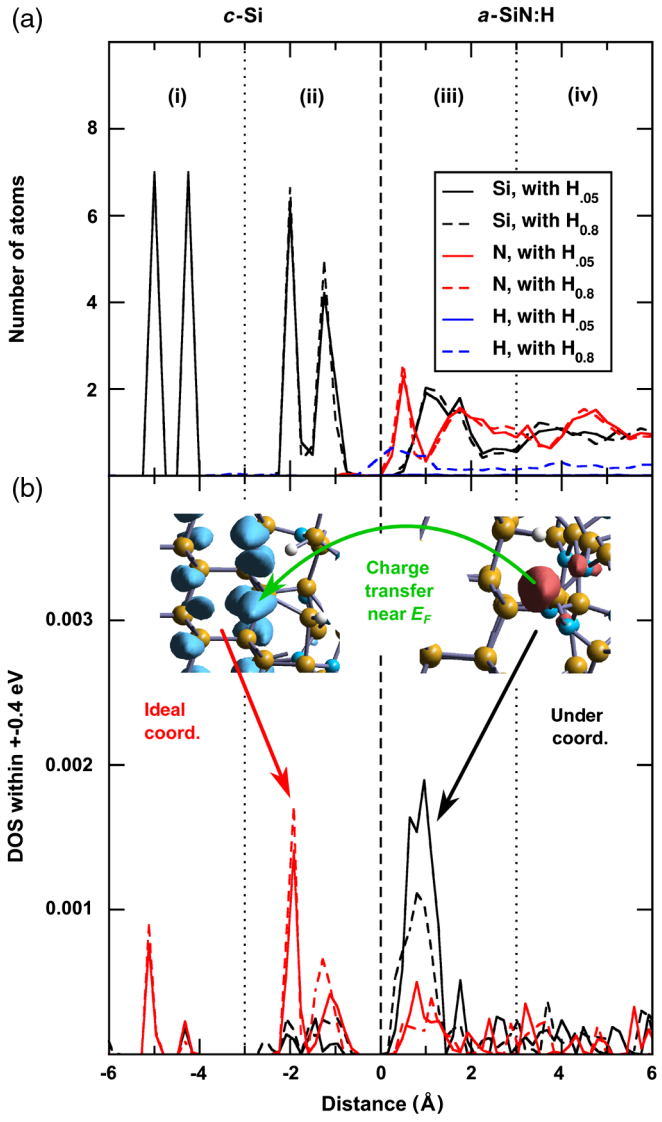

FIG. 1. (a) Number densities and (b) layer-resolved density of states (DOS) at the c-Si/a-$Si_3N_{3.5}$:H interfaces with 1- and 11-at. % H (solid and dashed lines, respectively). (a) The N number density shows a peak close to the interface integrating to 60% of the number density in the topmost Si layer. (b) The considered electronic states lie within ±0.4 eV of the Fermi level. The states are found to be predominantly localized either at atoms with ideal coordination or undercoordination (red or black arrow). These states are related to the conduction band of c-Si or to undercoordinated Si atoms in a-$Si_3N_{3.5}$:H. In some microscopic models, a charge transfer from occupied coordination defects (red isosurface) to the Si conduction band (blue isosurface) occurs (green arrow).

One central finding is that charge is partially transferred from originally occupied K defects in the a-SiN:H to the c-Si conduction band. This happens in about 7% of our microscopic models (green arrow). The opposite, a charge transfer from the c-Si valence band to originally unoccupied K^+ defects never occurs. The reason why only a small number of samples show this behavior is twofold. First, many of our interfaces are essentially defect-free. Second, if K defects are present at the interface, then the electronic levels of doubly occupied K^- defects are usually below the conduction band of c-Si, and the electronic levels of unoccupied K^+ defects are always well above the conduction-band edge of c-Si. Hence, in most models, no charge transfer occurs. Only in those rare cases, where a doubly occupied K^- defect is close or above the conduction band of c-Si, a charge transfer to the c-Si part can occur. In other words, the transfer of charge from K^- defects to Si is statistically rather unlikely and occurs only in 7% of the microscopic models. This also emphasizes that one needs many microscopic samples to obtain statistically meaningful results. Note that this result also correlates well with the experimental observation of a rather low defect concentration at c-Si/a-SiN:H interfaces.

Concerning H, we find that if H is present, the number density of H is clearly increased in the a-SiN:H part at the interface [Fig. 1(a), blue line], but the N and Si number densities are hardly changed. Although H reduces the number of midgap defect levels at the interface almost by a factor of 2 [Fig. 1(b), solid and dashed black lines), our general observations remain unchanged.

B. Band structure and defect levels

We now investigate three exemplary microscopic models in more detail. The first, sample A, contains a single localized doubly occupied K^- defect in the middle of the gap (Fig. 2). In addition to the band structure of sample A,

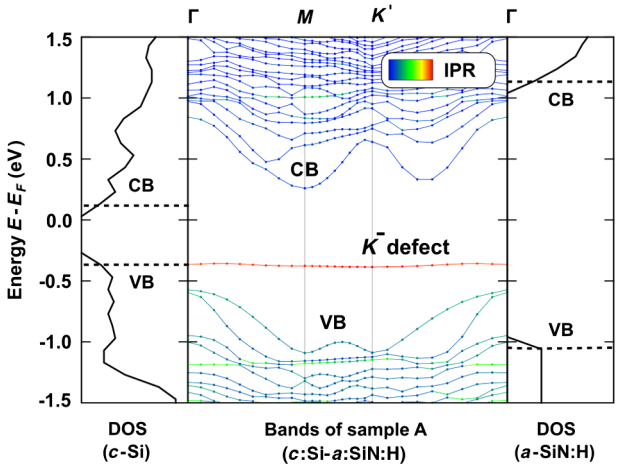

FIG. 2. Typical band structure and DOS of a c-Si/a-$Si_3N_{3.5}$:H interface sample in the presence of a single defect state. The color coding indicates the degree of localization and corresponds to the inverse participation ratio (IPR, red for localized states). Additionally, we show the DOS of a bulk undoped c-Si and a defect-free bulk a-$Si_3N_{3.5}$:H sample. In the band structure of the interface sample, the valance band (VB) and the conduction band (CB) can be determined by means of the IPR. For the bulk samples, the valance band maximum and the conduction band minimum are indicated. Note that E_F refers to the average Fermi level of the interface models.

we show the DOS of bulk undoped c-Si and a defect-free bulk a-SiN:H model structure (Fig. 2, left- and right-most panels, respectively). These bulk states are aligned at the 1s core levels of the Si and the N atoms in the middle of the c-Si and a-SiN:H parts, respectively. The comparison of the bulk DOS shows that the indirect band gap of c-Si (about 0.5 eV) is much smaller than the band gap of a-SiN:H (about 2.3 eV), and the conduction-band offset (about 1.0 eV) is larger than the valence-band offset (about 0.8 eV). That the band gaps are too small compared to experiment is a well-known DFT artifact; however, as shown, for instance, in Ref. [17], this error changes the midgap levels, which are particularly relevant for this study, only very little. The present offsets are consistent with photoemission experiments and previous simulations on c-Si/c-Si_3N_4 interfaces [17,29]. The band structure, furthermore, demonstrates that the in-plane dispersion of the defect level is negligible. This indicates that the lateral supercell size is generally sufficient, as there is no interaction between the periodically repeated defect images. However, the valence band and the conduction band of c-Si show a strong dispersion necessitating a dense 8×8 k-point sampling parallel to the interface.

Since defect-related states in the amorphous part can be situated anywhere within the gap of a-SiN:H [25], they often overlap with the c-Si conduction band or valence band. To give examples for such situations, we show the band structure of two samples B and C (Fig. 3). In sample B, a doubly occupied K^- defect merges into the c-Si valence band, and, in sample C, an initially doubly occupied K^- defect merges into the c-Si conduction band. In both samples, the defect states are again strongly localized and practically flat. Nevertheless, since small hybridizations between the c-Si and the defect level exist, forbidden crossings are observed. The most interesting case is sample C. Here the average defect level is slightly above the conduction-band minimum of c-Si, causing a partial transfer of charge from the defect level into the c-Si conduction band. This charge transfer has reduced the occupancy (OCC) of the defect from K^- to K^0 and relates to the main finding mentioned above. The opposite, a partial transfer from the c-Si valence band to an originally empty K^+ defect, is never observed. In other words, double-occupied K^- defects can be positioned above the conduction band. They then act as donors, donating charge to the crystalline Si. Unoccupied K^+ defects are always way above the valence band and can, therefore, never act as acceptors.

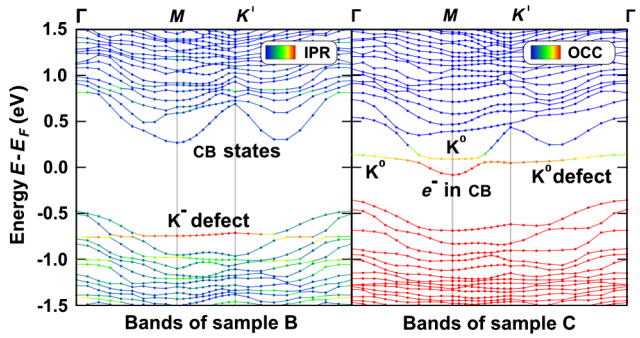

FIG. 3. Two examples for occupied K defects. In sample B, the defect level is close to the valence band, whereas, in sample C, it is close to the conduction band (CB). In sample C, a partial charge transfer into the conduction band is observed. Both defect states interact with the valence- or conduction-band states resulting in forbidden crossings.

C. Electronic states in the band gap

To obtain a statistically meaningful result, we now explore the electronic density of states evaluated close to the interface and averaged over all 90 samples (Fig. 4). On the c-Si side, we observe a slight band tailing introduced by local disorder and distorted Si bonds (red lines). However, the majority of the gap states are caused by undercoordinated Si atoms at the a-SiN:H side of the interface (black lines). The most important observation is that the minimum of the DOS of c-Si is shifted towards lower-energy values (left) in comparison to the minimum of the DOS of a-SiN:H. Likewise, the midgap energy level of bulk c-Si (red vertical line)—evaluated by taking the mean value of the valence-band maximum and conduction-band minimum of bulk Si—lies about 0.2 eV below the average Fermi level of bulk a-SiN:H (black vertical line). Impaired by the issue of too-small DFT band gaps, we believe that we observe only the lower bound of this offset here. Note that we have again taken the core levels of Si and N as

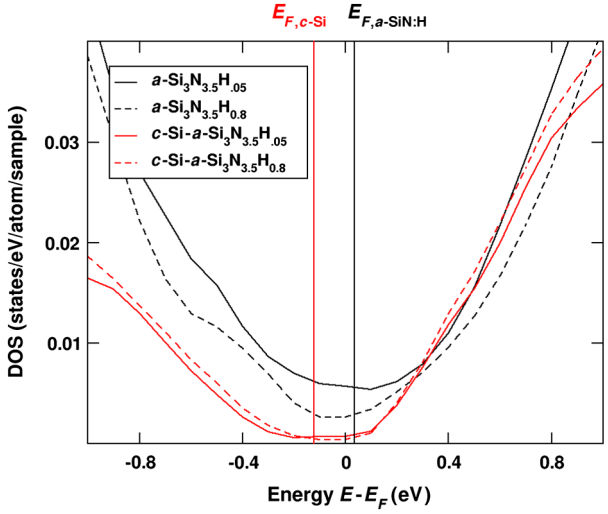

FIG. 4. Local electronic density of states evaluated for the c-Si part and for the a-SiN:H part (red or black lines) of the c-Si/a-$Si_3N_{3.5}$:H interfaces with 1- and 11-at. % H (solid and dashed lines, respectively). The midgap level of bulk c-Si and the Fermi level of a-$Si_3N_{3.5}H_{0.8}$ are shown by vertical lines in the corresponding colors.

reference for the alignment, and the general observations apply independently of the H concentration. As for our previous studies on bulk a-SiN:H [24,25], H mainly reduces the number of defects, although here it also slightly reduces the misalignment of the Fermi levels from 0.24 to 0.16 eV.

The offset of the midgap level of Si and the Fermi level of a-SiN:H has important consequences. In a macroscopic sample, the Fermi levels must align, and, in a real device, the alignment will occur via charge transfer from donors, here doubly occupied K^- defects in a-SiN:H, to acceptor levels in c-Si as illustrated in Fig. 5. In our microscopic realizations, this alignment is not strictly so, since the Fermi level of the c-Si part can be located anywhere between the conduction band and valence band: in the absence of acceptors and donors, the c-Si part does not pin the Fermi-level midgap. Only if an occupied K^- defect is located above the conduction band of c-Si, a partial charge transfer to the c-Si part is observed, like in the previous discussed sample C (see Fig. 3). This partial charge transfer shifts the c-Si states upwards and the a-SiN:H states downwards. This line of thought indicates that it is not quite straightforward to determine highly accurate conduction-band and valence-band offsets between amorphous model structures and crystalline samples by using small model structures, even though we average over many microscopic models. That the midgap level of c-Si lies well below the Fermi level of a-SiN:H is, however, a robust feature corroborated by three independent observations: (i) the observation of microscopic models with charge transfer to c-Si, (ii) the visual misalignment of the minima in the electronic DOS, and (iii) the misalignment of the calculated c-Si midgap level and the Fermi level of a-SiN:H.

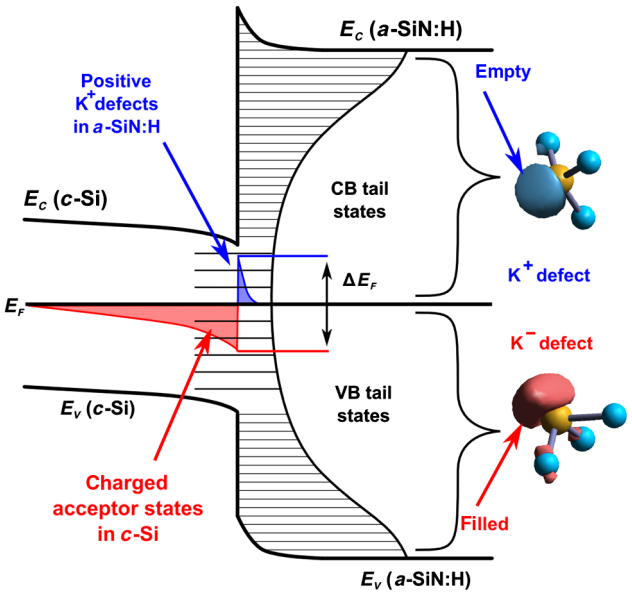

FIG. 5. Illustration of the predicted band bending at the c-Si/a-SiN:H interface. Before bringing both subsystems in contact, the midgap level of c-Si lies below the Fermi level of a-SiN:H (offset between the red and blue lines at the interface). In a-SiN:H, nearly all defect levels below and above the Fermi level are doubly occupied K^- defects and unoccupied K^+ defects, respectively. Only a few singly occupied K^0 defects are located at the Fermi level. To align the Fermi levels, K^- and K^0 defects donate charge to shallow acceptor levels in c-Si (red area). They are thereby converted to K^0 and K^+ defects (blue area).

IV. CONCLUSIONS

In summary, we conclude that the number of under-coordinated Si atoms (K defects) is significantly increased at c-Si/a-SiN:H interfaces compared to bulk a-SiN:H [compare Fig. 1(b)]. We try to find simple models explaining this observation but find no conclusive explanation. It is simply a result of the structural mismatch between c-Si and a-SiN:H. Remarkably, the structure of the interface is changed very little in the presence of H. However, H reduces the number of coordination defects and related electronic defect states by about a factor of 2 in our simulation. Similar to bulk a-SiN:H, H clearly cures geometrical defects at the interface by forming a bond to otherwise threefold-coordinated K defects. This parallels the experimental observation that H drastically reduces the number of electronically active defects in a-SiN:H and at c-Si/a-SiN:H interfaces.

The most important finding, however, is that we predict a positive, fixed charge at the c-Si/a-SiN interfaces. Our model calculations suggest that the fixed charge originates from a partial transfer of charge from otherwise doubly occupied K^- defects to the conduction band of c-Si, converting these defects to approximately neutral K^0 defects. In a real device, the charge transferred to the conduction band will screen the positive charge at the interface (compare Fig. 5). The origin for this partial charge transfer is intimately related to our observation that the midgap level of bulk c-Si lies about 0.2 eV below the Fermi level of bulk a-SiN:H. Consequently, in a real device, electrons will be transferred from originally doubly occupied K^- defects on the a-SiN:H side, to acceptor levels on the c-Si side in order to align the Fermi level in the heterostructure. Solving the Poisson equation for this standard device problem results in a band bending at the interface (indicated by black lines in Fig. 5). Clearly, such a band bending will attract electrons to the interface aiding the electron removal by metallic leads, which are etched into the a-SiN:H. Holes, on the other hand, are repelled, making an effective separation of both carriers possible. Concerning the precise offset of the midgap levels of 0.2 eV, we need to reiterate here that we believe that this is a lower bound of the real value. Specifically, we observe many microscopic models, in which doubly occupied K^- states lie well above or align with the conduction band of c-Si. In these models, charge is *de facto* transferred from the a-SiN:H part to the c-Si part, reducing the mismatch of

the midgap levels. In our microscopic models, the Fermi level of *a*-SiN:H can, at best, align with the conduction band of *c*-Si. This situation sets a lower bound for the mismatch of the midgap level to about half the *c*-Si band gap in DFT (0.25 eV). Thus, the real misalignment, before bringing both materials in contact, can well be larger. We can express this observation also in a more affirmative manner: since doubly occupied K^- states overlap with the *c*-Si conduction band in many microscopic models, all our observations will hold even for strongly *n*-doped *c*-Si, where the *c*-Si Fermi level is just below the *c*-Si conduction band. Viewed from this point, our simulations suggest that the Fermi level of *a*-SiN:H lies somewhat above the conduction band of *c*-Si (before bringing both materials in contact). An inspection of the results for accurate quasiparticle calculations for *c*-Si/Si_3N_4 interfaces confirms this. Both in DFT and in the quasi particle calculations, the midgap level of crystalline Si_3N_4 lies about 0.6 eV above the conduction band of *c*-Si (compare Fig. 6 in Ref. [17]).

A second important insight of our study is that the number of K defects and the amount of positive charge at the interface are interrelated quantities. If the defect density is very low, there will simply be very few defects that can donate charge to the *c*-Si part. The resulting lack of positively charged defects will thus reduce the positive interface charge and the band bending. If the defect density is high, the fixed charge density will be high, but more recombination centers will be present at the interface as well. These results are exactly in line with recent experimental studies [10,19]. In other words, it is not possible to reduce the density of carrier traps (K^-, K^0, and K^+ defects) without changing the field-effect passivation of fixed charges, as the species responsible for the fixed charges and K defects are identical.

Based on our present results, we suppose that it will be hard to achieve a negative, fixed charge by using the standard *a*-SiN:H passivation. This is certainly a somewhat disappointing result, but one that is, nevertheless, important. In order to achieve the (opposite) field-effect passivation for *p*-doped *c*-Si, the Fermi level of *a*-SiN:H must be lowered significantly. This feat seems to be almost impossible to achieve, since the Fermi level of *a*-SiN:H is essentially pinned by the presence of K^- and K^+ defects. If our results are correct, then the midgap level of *a*-SiN:H aligns with the conduction band of *c*-Si, and the Fermi level of *a*-SiN:H must be moved by at least the gap of *c*-Si (1.12 eV). We cannot see how this can possibly be achieved in a thermodynamically stable manner.

ACKNOWLEDGMENTS

This work is part of the HiperSol (high performance solar cells) project funded by the European commission Grant No. MMP3-SL-2009-228513. Supercomputing time on the Vienna Scientific Cluster is gratefully acknowledged.

[1] A. Luque and S. Hegedus, *Handbook of Photovoltaic Science and Engineering* (Wiley, New York, 2011).
[2] D. Abou-Ras, T. Kichart, and U. Rau, *Advanced Characterization Techniques for Thin Film Solar Cells* (Wiley, New York, 2011).
[3] M. A. Green, K. Emery, Y. Hishikawa, W. Warta, and E. D. Dunlop, Solar cell efficiency tables (version 39), Prog. Photovoltaics **20**, 12 (2012).
[4] A. G. Aberle, Surface passivation of crystalline silicon solar cells: A review, Prog. Photovoltaics **8**, 473 (2000).
[5] F. Duerinckx and J. Szlufcik, Defect passivation of industrial multicrystalline solar cells based on PECVD silicon nitride, Sol. Energy Mater. Sol. Cells **72**, 231 (2002).
[6] W. Shockley and W. T. Read, Statistics of the recombinations of holes and electrons, Phys. Rev. **87**, 835 (1952).
[7] R. N. Hall, Electron-hole recombination in germanium, Phys. Rev. **87**, 387 (1952).
[8] R. H. Bube, *Fundamentals of Solar Cells: Photovoltaic Solar Energy Conversion* (Academic, New York, 1983).
[9] M. A. Green, *Solar Cells: Operating Principles, Technology and System Applications* (University of New South Wales, Englewood Cliffs, 1986).
[10] M. W. P. E. Lamers, K. T. Butler, J. H. Harding, and A. Weeber, Interface properties of *a*-SiN_x:H/Si to improve surface passivation, Sol. Energy Mater. Sol. Cells **106**, 17 (2012).
[11] A. G. Aberle, Overview on SiN surface passivation of crystalline silicon solar cells, Sol. Energy Mater. Sol. Cells **65**, 239 (2001).
[12] J. Robertson, W. L. Warren, and J. Kanicki, Nature of the Si and N dangling bonds in silicon nitride, J. Non-Cryst. Solids **187**, 297 (1995).
[13] A. Omeltchenko, M. E. Bachlechner, A. Nakano, R. K. Kalia, P. Vashishta, I. Ebbsjö, A. Madhukar, and P. Messina, Stress Domains in Si(111)/*a*-Si_3N_4 Nanopixel: Ten-Million-Atom Molecular Dynamics Simulations on Parallel Computers, Phys. Rev. Lett. **84**, 318 (2000).
[14] M. Yang, R. Q. Wu, W. S. Deng, L. Shen, Z. D. Sha, Y. Q. Cai, Y. P. Feng, and S. J. Wang, Electronic structures of β-Si_3N_4(0001)/Si(111) interfaces: Perfect bonding and dangling bond effects, J. Appl. Phys. **105**, 024108 (2009).
[15] K. T. Butler, M. P. W. E. Lamers, A. W. Weeber, and J. H. Harding, Molecular dynamics studies of the bonding properties of amorphous silicon nitride coatings on crystalline silicon, J. Appl. Phys. **110**, 124905 (2011).
[16] K. T. Butler, J. H. Harding, M. P. W. E. Lamers, and A. W. Weeber, Stoichiometrically graded SiN_x for improved surface passivation in high performance solar cells, J. Appl. Phys. **112**, 094303 (2012).
[17] E. Flage-Larsen, O. M. Løvvik, C. M. Fang, and G. Kresse, β-Si_3N_4(0001)/Si(111) interface: Phosphorus defects, valence band offsets, and their role of passivating the interface states, Phys. Rev. B **88**, 165310 (2013).
[18] M. W. P. E. Lamers, K. T. Butler, P. E. Vullum, J. H. Harding, and A. Weeber, Characterization of *a*-SiN_x:H layer: Bulk properties, interface with Si and solar cell efficiency, Phys. Status Solidi (a) **210**, 658 (2013).
[19] Machteld Lamers, L. E. Hintzsche, K. T. Butler, P. E. Vullum, C. M. Fang, M. Marsman, G. Jordan, J. H. Harding,

G. Kresse, and A. Weeber, The interface of *a*-SiN_x:H and Si: Linking the nano-scale structure to passivation quality, Sol. Energy Mater. Sol. Cells **120**, 311 (2014).

[20] T. Anh Pham, T. Li, H. V. Nguyen, S. Shankar, F. Gygi, and G. Galli, Band offsets and dielectric properties of the amorphous $Si_3N_4/Si(100)$ interface: A first-principles study, Appl. Phys. Lett. **102**, 241603 (2013).

[21] P. E. Blöchl, Projector augmented-wave method, Phys. Rev. B **50**, 17953 (1994).

[22] J. Furthmüller, J. Hafner, and G. Kresse, *Ab initio* calculation of the structural and electronic properties of carbon and boron nitride using ultrasoft pseudopotentials, Phys. Rev. B **50**, 15606 (1994).

[23] G. Kresse and J. Furthmüller, Efficient iterative schemes for *ab initio* total-energy calculations using a plane-wave basis set, Phys. Rev. B **54**, 11169 (1996).

[24] L. E. Hintzsche, C. M. Fang, T. Watts, M. Marsman, G. Jordan, M. W. P. E. Lamers, A. W. Weeber, and G. Kresse, Density functional theory study of the structural and electronic properties of amorphous silicon nitrides: Si_3N_{4-x}:H, Phys. Rev. B **86**, 235204 (2012).

[25] L. E. Hintzsche, C. M. Fang, M. Marsman, G. Jordan, M. W. P. E. Lamers, A. W. Weeber, and G. Kresse, Defects and defect healing in amorphous $Si_3N_{4-x}H_y$: An *ab initio* density functional theory study, Phys. Rev. B **88**, 155204 (2013).

[26] J. P. Perdew, A. Ruzsinszky, G. I. Csonka, O. A. Vydrov, G. E. Scuseria, L. A. Constantin, X. Zhou, and K. Burke, Restoring the Density-Gradient Expansion for Exchange in Solids and Surfaces, Phys. Rev. Lett. **100**, 136406 (2008).

[27] S. Nosé, A unified formulation of the constant temperature molecular dynamics methods, J. Chem. Phys. **81**, 511 (1984).

[28] W. G. Hoover, Canonical dynamics: Equilibrium phase-space distributions, Phys. Rev. A **31**, 1695 (1985).

[29] R. Kärcher, L. Ley, and R. L. Johnson, Electronic structure of hydrogenated and unhydrogenated amorphous $SiN_x(0 \leq x \leq 1.6)$: A photoemission study, Phys. Rev. B **30**, 1896 (1984).